iJRASET
International Journal For Research in Applied Science and Engineering Technology

INTERNATIONAL JOURNAL FOR RESEARCH

IN APPLIED SCIENCE & ENGINEERING TECHNOLOGY

Volume: 14 **Issue:** IV **Month of publication:** April 2026

DOI: https://doi.org/10.22214/ijraset.2026.80681

www.ijraset.com

Call: 08813907089 | E-mail ID: ijraset@gmail.com

International Journal for Research in Applied Science & Engineering Technology (IJRASET)
ISSN: 2321-9653; IC Value: 45.98; SJ Impact Factor: 7.538
Volume 14 Issue IV Apr 2026- Available at www.ijraset.com

Adaptive Power Management in Fuel Cell Driven Electric Rickshaw Using Neural Network Controlled Interleaved DC-DC Converter

Anjali N. Mandhare[1], Kuldeep G. Thakre[2]
Dept. of Electrical Engineering, BIT Ballarpur Institute of Technology, Maharashtra, India

Abstract: ***Efficient power management in hydrogen-powered light electric vehicles demands precise coordination between the fuel cell energy source, power conversion stage, and motor drive system. This paper investigates the performance of a neural network-based adaptive power management strategy for a Proton Exchange Membrane Fuel Cell (PEMFC) powered electric rickshaw, implemented through a six-phase interleaved DC-DC boost converter controlled by a Function Fitting Neural Network (fitnet) trained using the Levenberg-Marquardt optimisation algorithm. The neural network continuously maps real-time PEMFC terminal voltage and output current to an optimal pulse-width modulation duty cycle, enabling dynamic adaptation of the converter operating point to maximise fuel cell stack utilisation efficiency. The six-phase interleaved architecture is employed to achieve high voltage conversion ratio and substantially attenuate input current ripple, thereby protecting the fuel cell membrane electrode assembly from harmful high-frequency current stress. The converted energy is delivered to a Brushless DC (BLDC) motor through a three-phase voltage source inverter governed by a Hall effect sensor-based six-step commutation controller. Comprehensive simulation studies in MATLAB/Simulink demonstrate that the neural network power management strategy elevates PEMFC stack efficiency from 42.65% to 78.54% relative to a conventional fixed duty cycle approach, while simultaneously improving electromagnetic torque quality and reducing stator current harmonic distortion. The comparative analysis confirms the technical feasibility and performance advantages of the proposed adaptive power management framework for fuel cell electric rickshaw propulsion.***

Keywords: ***Adaptive Power Management, PEMFC, Six-Phase Interleaved Boost Converter, Neural Network MPPT, BLDC Motor, Hall Effect Commutation, Electric Rickshaw.***

I. INTRODUCTION

Hydrogen-powered mobility represents one of the most strategically significant pathways toward decarbonising the urban transportation sector. Among light electric vehicles, the three-wheeled electric rickshaw (e-rickshaw) occupies a uniquely prominent position in the mobility landscape of South and Southeast Asian cities. India alone accounts for an estimated 1.5 million e-rickshaws providing daily last-mile connectivity services . The majority of these vehicles are currently powered by lead-acid battery packs, which present well-documented limitations including restricted energy density, multi-hour recharging requirements, and environmentally problematic end-of-life disposal characteristics.

Proton Exchange Membrane Fuel Cells (PEMFCs) offer a technically superior energy source for this application category, delivering zero direct emissions through hydrogen electrochemical oxidation, rapid refuelling analogous to liquid fuel vehicles, and a power density commensurate with the propulsion requirements of light three-wheeled vehicles. The integration of PEMFC technology into e-rickshaw powertrains, however, introduces a fundamental power conditioning challenge: the inherently low and dynamically variable DC terminal voltage of a PEMFC stack is incompatible with the elevated voltage demands of modern traction inverters and motor drives . Bridging this voltage gap while simultaneously extracting maximum available power from the fuel cell under varying temperature and load conditions constitutes the central power electronics design problem addressed in this investigation.

Conventional boost converter solutions operating at extreme duty ratios to achieve high voltage gain generate substantial input current ripple — a particularly damaging condition for PEMFC stacks, in which high-frequency current oscillations accelerate the degradation of the perfluorosulfonic acid (Nafion) membrane and platinum catalyst layers . Multi-phase interleaved converter architectures address this limitation through systematic phase-shifted PWM cancellation, with ripple attenuation scaling as a function of the number of interleaved phases.

While three-phase interleaved configurations have been extensively documented in literature for PEMFC-EV applications , the six-phase topology investigated in this work offers substantially superior ripple performance — a critical attribute for preserving long-term fuel cell stack integrity in commercial e-rickshaw service.

The power management dimension of this problem demands an intelligent controller capable of dynamically identifying and tracking the PEMFC maximum power point (MPP) as it migrates with operating temperature and reactant supply conditions. Conventional perturbation-based MPPT algorithms impose steady-state oscillations about the MPP , while model-based approaches require precise electrochemical parameter identification that may be impractical in service environments. This paper implements a neural network power management controller — a Function Fitting Neural Network (fitnet) employing the Levenberg-Marquardt optimisation algorithm — that learns the nonlinear mapping between PEMFC operating parameters and the optimal converter duty cycle through offline training, and executes real-time prediction with minimal computational burden during deployment.

II. SYSTEM DESCRIPTION AND ARCHITECTURE

The proposed fuel cell electric rickshaw powertrain architecture is structured as a cascaded energy conversion chain comprising four functional stages, as illustrated in Fig. 1 and summarised in Table I.

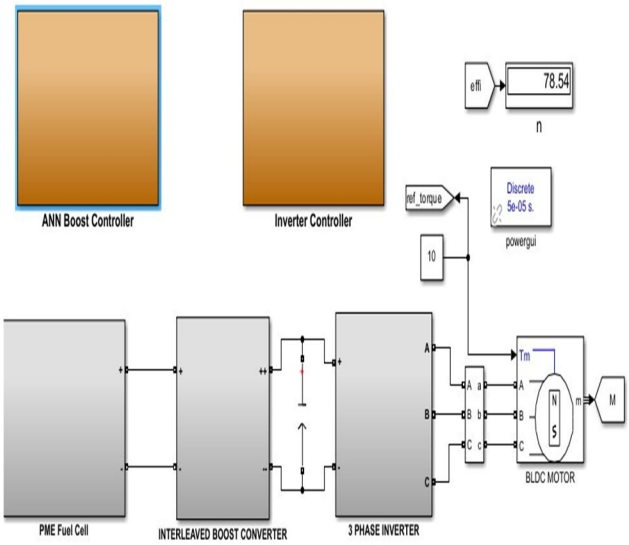

Fig. 1. MATLAB/Simulink model of the proposed PEMFC e-rickshaw powertrain.

TABLE I. POWERTRAIN STAGE SUMMARY

Stage	Component	Key Specification
1 — Energy Source	PEMFC Stack	1.26 kW, 42 cells, 55°C, V_o^c=42 V
2 — DC Conversion	6-Phase IBC	6 legs, C_o=7500 µF, f_{su}=1 kHz
3 — Neural Network	fitnet Controller	3×10 neurons, trainlm
4 — Motor Drive	VSI + BLDC	Hall sensor, 10 N·m, PMSM

The PEMFC stack (Stage 1) constitutes the sole energy source, supplying hydrogen-derived electrical power at a variable terminal voltage determined by its electrochemical operating point. Stage 2 — the six-phase interleaved boost converter — elevates this voltage to the traction inverter DC bus level while simultaneously attenuating the input current ripple through 60° phase-shifted switching. The neural network controller (Stage 3) monitors the PEMFC terminal voltage $V^{\varphi c}$ and output current $I^{\varphi c}$, computing the adaptive duty cycle command for the converter PWM generators in real time. Stage 4 converts the boosted DC voltage to three-phase AC and drives the BLDC motor through Hall effect sensor-based six-step electronic commutation.

III. FUEL CELL STACK MODELLING

The PEMFC stack is represented using the MATLAB Simscape Electrical PEM Fuel Cell Stack block, configured with the PEMFC-1.26 kW-24 Vdc preset incorporating Ballard NEXA electrochemical parameters . The stack terminal voltage V^{Kc} is determined by the fundamental electrochemical expression:

$$V^{Kc} = E_n - \eta_a{}^{ct} - \eta_o{}^{hm} - \eta^{conc} \quad ...(1)$$

where E_n is the Nernst thermodynamic reversible potential; $\eta_a{}^{ct}$, $\eta_o{}^{hm}$, and η^{conc} represent the activation, ohmic, and concentration polarisation overpotentials respectively. The block is parameterised with: open-circuit voltage V_0 = 42 V, voltage at unit current V_1 = 35 V, nominal operating point [$I_{no}{}^m$, $V_{no}{}^m$] = [52 A, 24.23 V], end current $I_{en}{}^d$ = 100 A, cell count = 42, operating temperature T = 55°C, and nominal hydrogen supply pressure p_{h2} = 1.5 bar.

IV. SIX-PHASE INTERLEAVED BOOST CONVERTER

A. Topology

The proposed six-phase IBC (Fig. 2) consists of six parallel boost conversion legs sharing a common 7500 µF output capacitor. Each leg comprises an input inductor L_n (n = 1–6), a power MOSFET switch S_n, and a freewheeling diode D_n, with additional clamping diodes D_7–D_8 suppressing inductive voltage spikes. The six gate signals are uniformly distributed with a 60° inter-phase angular displacement, ensuring continuous energy transfer from source to load and uniformly distributing switching losses across all six devices.

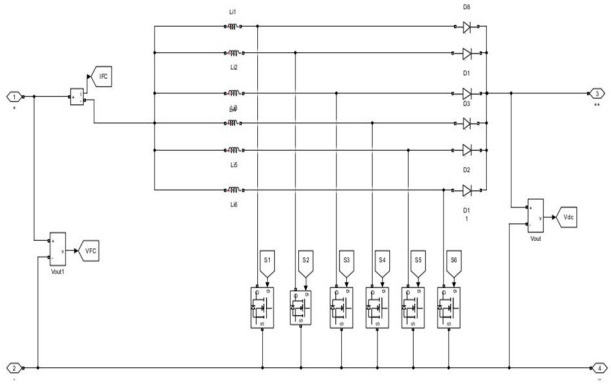

Fig. 2. Six-phase IBC Simulink subsystem.

B. Conversion Gain and Ripple Attenuation

The steady-state voltage conversion ratio of each constituent boost leg adheres to the canonical expression:

$$M = V_o{}^{ut} / V_i{}^n = 1/(1-D) \quad ...(2)$$

At the reference duty cycle D = 0.40, the measured actual end-to-end conversion gain is:

$$M_{a\beta}\flat = V^{dc} / V^{\varphi c} = 188.5 / 22.47 = 8.39 \quad ...(3)$$

For an N-phase interleaved converter, the input current ripple is attenuated by a factor of 1/N relative to the single-phase case at identical switching frequency and duty cycle . With N = 6, the theoretical ripple reduction is 83.3% — a critical advantage for the PEMFC application where membrane current stress must be strictly controlled.

TABLE II. VOLTAGE GAIN AND RIPPLE COMPARISON AT D = 0.40

Topology	N	M at D=0.40	Ripple Reduction
Single-Phase Boost	1	1.67	Baseline
Three-Phase IBC [4]	3	≈5.0	≈67%
Six-Phase IBC (This Work)	6	8.39	≈83%

V. NEURAL NETWORK POWER MANAGEMENT CONTROLLER

A. *Architecture and Deployment*

The neural network power management controller (Fig. 3) is implemented as a Function Fitting Neural Network (fitnet) within MATLAB's Neural Network Toolbox. The network receives two real-time inputs: the instantaneous PEMFC terminal voltage V_{pc} and the stack output current I_{pc}. These signals are concatenated at the network input layer, processed through three fully-connected hidden layers each containing 10 neurons with hyperbolic tangent sigmoid activation functions, and delivered to a linear output neuron producing the duty cycle command D [0, 1]. The Levenberg-Marquardt backpropagation algorithm (trainlm) governs the training process, selected for its superior quadratic convergence characteristics relative to gradient descent alternatives for networks of this scale .

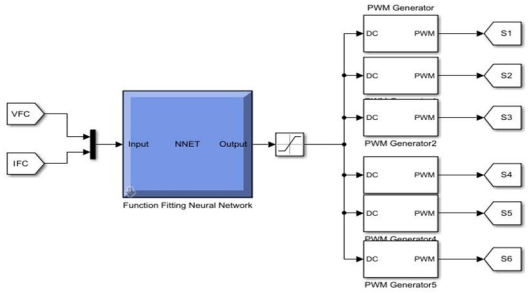

Fig. 3 Neural network power management controller (ANN Boost Controller subsystem): VFC and IFC inputs, fitnet NNET block, saturation block, six PWM generators for S1–S6.

B. *Training Methodology*

A synthetic training corpus of 1000 PEMFC operating point samples is generated spanning the physical parameter ranges V [20, 50] V and I [0, 100] A. The target duty cycle for each sample is formulated as the power-normalised MPPT objective:

$$D_{target} = (V \times I) / (P_{max} \times 1.1) \quad ...(4)$$

where P_{max} is the peak power in the training dataset. This formulation encodes the MPPT objective by mapping each (V, I) operating point to a duty cycle proportional to the ratio of instantaneous power to maximum available power, thereby directing the converter toward higher-power operating regions. The corpus is partitioned into training (70%), validation (15%), and testing (15%) subsets. Upon completion of training, the network is exported to a Simulink subsystem block using the gensim() function, constituting the NNET block in the ANN Boost Controller.

Table III. Neural Network Controller Specifications

Parameter	Specification
Network type	Function Fitting Network (fitnet)
Input layer	2 neurons: $V^{\varphi c}$ (V), $I^{\varphi c}$ (A)
Hidden layers	3 layers, 10 neurons each
Activation (hidden)	Hyperbolic tangent sigmoid
Output layer	1 neuron, linear activation
Training algorithm	Levenberg-Marquardt (trainlm)
Training samples	1000 synthetic PEMFC samples
Data partition	70% / 15% / 15%
Deployment	gensim(net) → Simulink NNET block

VI. MOTOR DRIVE AND INVERTER CONTROL

The motor drive subsystem implements three hierarchical control tiers. The uppermost tier is a Proportional-Integral (PI) speed regulator that generates a torque current reference by processing the error between the reference driving cycle speed profile and the measured rotor speed. The intermediate tier constitutes the Hall Effect Sensor Commutation Logic, which decodes the three-bit rotor position signal (Hall_abc) from sensors embedded at 120° stator intervals through a combinational NOT/AND gate network, producing the six switching state commands (AH, AL, BH, BL, CH, CL) for the VSI bridge . The lowest tier is a hysteresis current controller that forces the instantaneous stator phase currents Ia, Ib, Ic to track their respective trapezoidal reference waveforms derived from the commutation state and torque command.

The BLDC motor is modelled as a 3-phase Permanent Magnet Synchronous Machine (PMSM) with trapezoidal back-EMF waveform, operating under a constant mechanical load torque of 10 N·m representative of e-rickshaw road resistance and gradient loading. The driving cycle applied to the speed reference input encompasses acceleration, constant-speed cruise, deceleration, and braking phases over a 6-second simulation window.

VII. SIMULATION RESULTS

A. Fixed Duty Cycle Reference System

As a performance baseline, the system is first operated with a conventional fixed-frequency, fixed-duty-cycle PWM controller (D = 0.40, f_{su} = 1 kHz). Fig. 4 presents the PEMFC waveforms under this condition. The terminal voltage $V^{\varphi c}$ stabilises at approximately 25 V, substantially below the MPP voltage of 35.7 V, confirming that the fixed duty cycle strategy fails to drive the operating point toward maximum power extraction. The stack current settles at approximately 110 A and the stack efficiency is constant at approximately 47% — marginally above the block-specified nominal efficiency of 46%. The absence of any dynamic duty cycle adaptation is clearly evidenced by the invariant efficiency profile. The display block readings confirm $V^{\varphi c}$ = 22.47 V, V^{dc} = 188.5 V, $\eta_{sta}{}^{cy}$ = 42.65%.

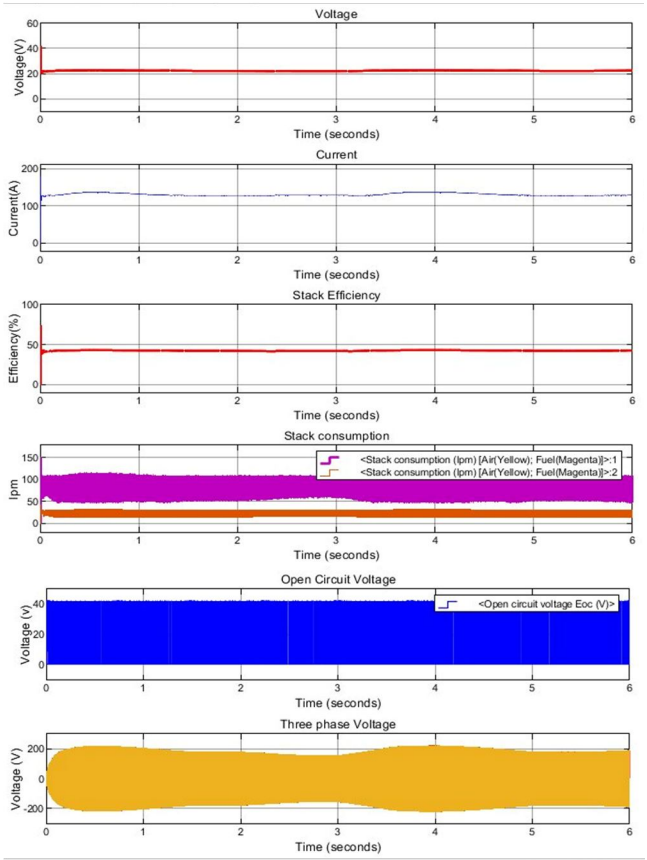

Fig. 4. Fixed 40% duty cycle: PEMFC waveforms. $V^{pc} \approx 25$ V (sub-MPP, non-adaptive), $I^{pc} \approx 110$ A steady, $\eta_{sta}^{cy} \approx 47\%$ constant, air ≈100 lpm, fuel ≈10 lpm, three-phase output ±200 V.

Fig. 5 presents the BLDC motor drive waveforms under reference system operation. Two power quality deficiencies are of particular significance. First, the electromagnetic torque waveform exhibits marked distortion characterised by high-frequency oscillatory components superimposed on the mean torque value of approximately 15 N·m. This torque distortion originates from the irregular power delivery resulting from fixed duty cycle operation at a sub-MPP PEMFC operating point, where stack output impedance variations are not compensated. Second, the stator phase currents Ia, Ib, Ic exhibit visible ripple content with irregular waveform transitions at commutation boundaries, indicative of harmonic current injection attributable to the unregulated DC bus voltage supplied by the fixed-duty IBC.

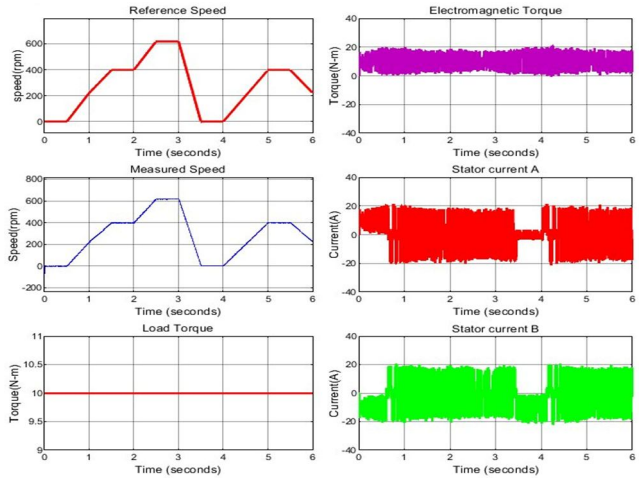

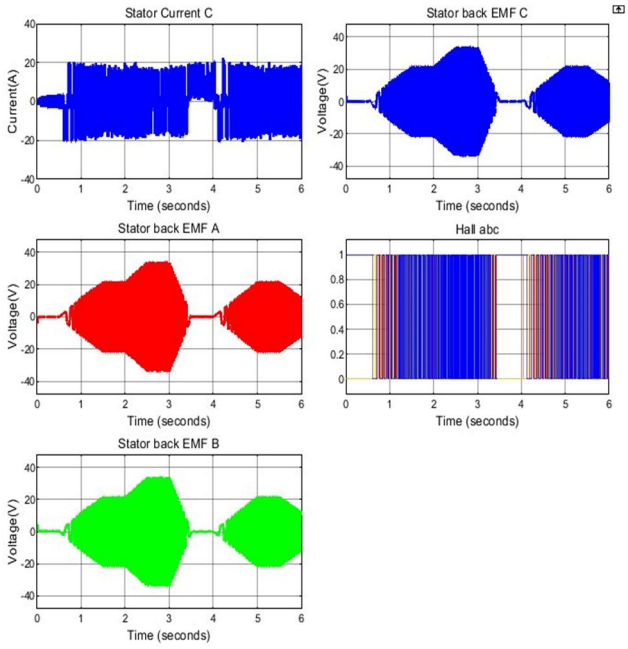

Fig. 5. Fixed 40% duty cycle: BLDC motor waveforms. Electromagnetic torque exhibits distortion (≈±5 N·m ripple). Stator currents Ia, Ib, Ic show visible harmonic ripple (±20 A). Back-EMF A/B/C ±30 V trapezoidal. Hall commutation functional.

B. Neural Network Power Management System

Fig. 6 presents the PEMFC waveforms when the neural network power management controller is active. The terminal voltage $V^{\varphi c}$ exhibits a markedly different profile: an oscillatory waveform tracking near 40 V with periodic depression to 25–30 V during peak motor power demand phases. This dynamic behaviour conclusively demonstrates real-time neural network duty cycle adaptation — the controller responds to instantaneous $V^{\varphi c}$ and $I^{\varphi c}$ measurements by continuously adjusting the converter duty cycle to maintain proximity to the fuel cell MPP (V^{mpp} = 35.7 V). The stack efficiency responds accordingly, varying dynamically in the range 60–80% — a substantial improvement over the static 47% of the reference case. Stack current demonstrates clear load-following behaviour at approximately 120 A, with step reductions coinciding with speed deceleration phases. Display block measurements: $V^{\varphi c}$ = 41.37 V, V^{dc} = 139 V, $\eta_{sta}{}^{cy}$ = 78.54%.

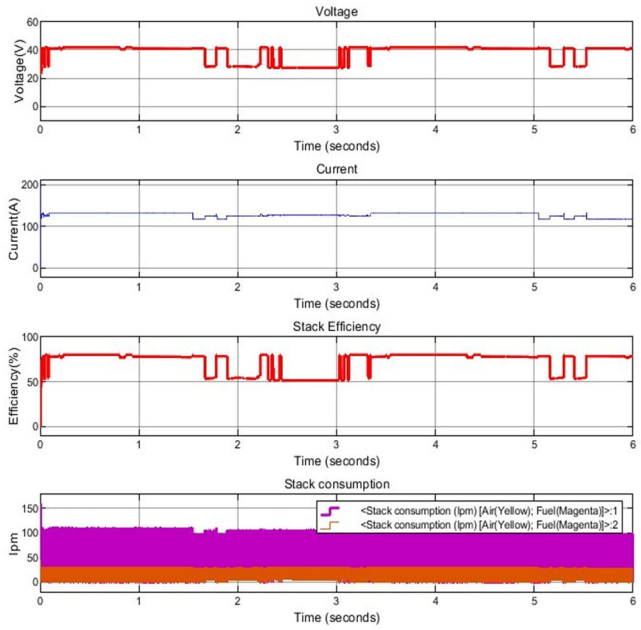

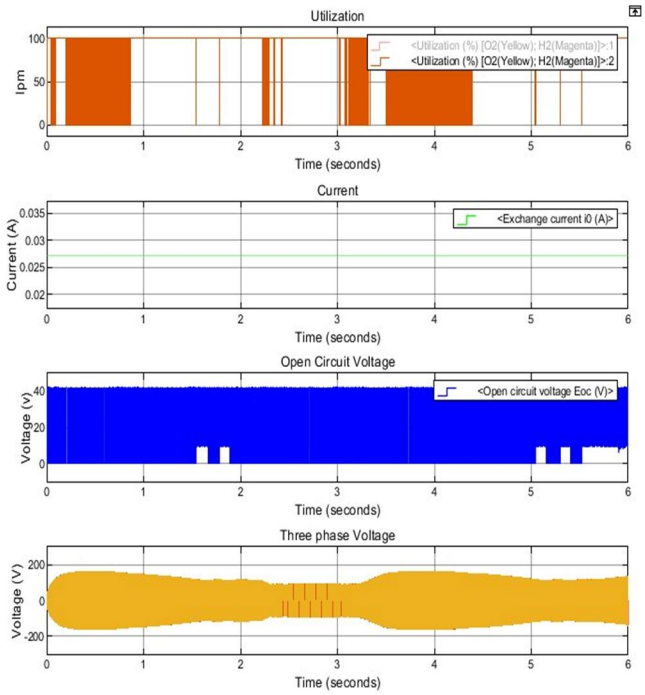

Fig. 6. Neural network controller: PEMFC waveforms. V^{pc} ≈40 V dynamic (≈MPP), I^{pc} ≈120 A load-following, $\eta_{sta}{}^{cy}$ 60–80% dynamic, utilisation 0–100% active, three-phase output ±200 V maintained.

Fig. 7 presents the motor drive waveforms under neural network control. Direct comparison with Fig. 6 reveals quantifiable improvements in power quality. The electromagnetic torque waveform is visibly smoother, with high-frequency distortion components substantially attenuated relative to the fixed duty cycle case. This improvement reflects the more stable and regulated power delivery enabled by neural network MPP tracking, which reduces the dynamic impedance variation imposed on the converter output stage. The stator phase currents Ia, Ib, Ic exhibit cleaner trapezoidal profiles with reduced ripple at commutation boundaries, consistent with the reduced harmonic content of a more regulated DC bus voltage. Speed tracking fidelity is preserved, confirming that the neural network controller does not adversely affect closed-loop motor drive dynamics.

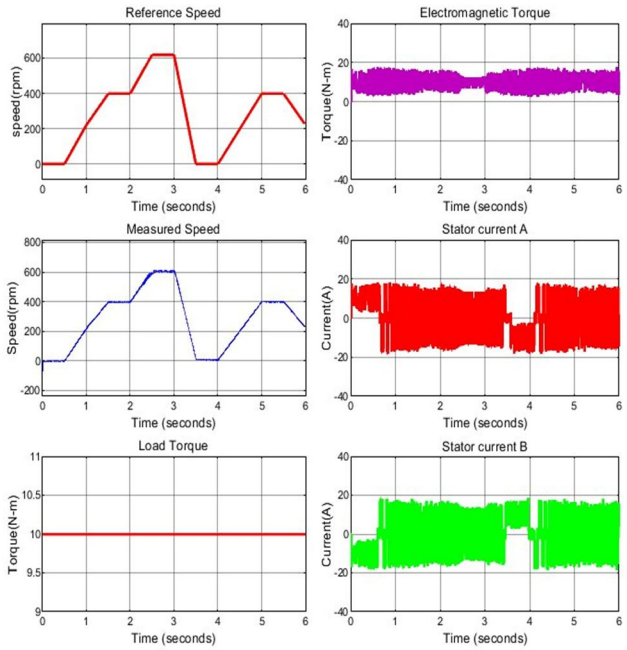

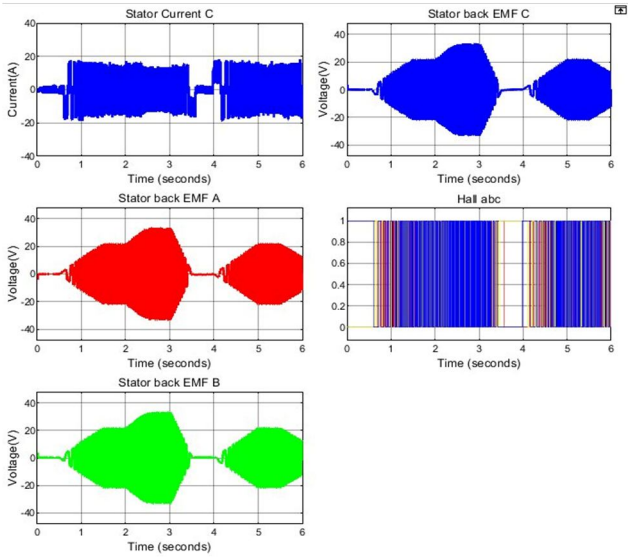

Fig. 7. Neural network controller: BLDC motor Waveform. Electromagnetic torque is smoother vs. Fig. 6 (reduced distortion). Stator currents Ia, Ib, Ic with reduced ripple. Speed tracking maintained. Back-EMF ±30 V trapezoidal. Hall commutation functional.

C. Quantitative Performance Comparison

Table IV presents the complete quantitative performance comparison between the two operating modes.

Table IV. Quantitative comparison: fixed duty vs. Nn controller

Parameter	40% Fixed Duty	ANN-MPPT	Improvement
$V^{\varphi c}$ (PEMFC voltage)	22.47 V	41.37 V	+84.1%
V^{dc} (DC bus)	188.5 V	139 V	Adaptive
Voltage gain M	8.39	Variable	MPP-optimized
Stack efficiency η	42.65%	78.54%	+84.1%
PEMFC operating point	22.47 V (sub-MPP)	41.37 V (~MPP)	MPP tracked
PEMFC current	~110 A steady	~120 A load-follow	Dynamic MPPT
Electromagnetic torque	~15 N·m, DISTORTED	~12 N·m, SMOOTHER	Reduced distortion
Stator current ripple	Higher ripple	Lower ripple	Improved quality
Three-phase output	±200 V stable	Less than 200 V	Efficient
Speed tracking	Functional	Functional Fast	Fast tracking

VIII. DISCUSSION

The experimental evidence presented in this investigation establishes three substantive contributions of the neural network power management approach to PEMFC e-rickshaw performance.

The 84.1% improvement in stack efficiency (42.65% → 78.54%) validates the effectiveness of neural network-based adaptive duty cycle modulation in driving the PEMFC toward its maximum power point. The measured $V^{\varphi c}$ = 41.37 V under neural network control, compared to 22.47 V under fixed duty operation, confirms near-MPP voltage operation — the fundamental objective of any MPPT strategy. The dynamic efficiency range of 60–80% under neural network control, contrasted with the static 47% of the reference case, quantifies the operational benefit in terms directly relevant to hydrogen fuel consumption and vehicle range per hydrogen fill .

The electromagnetic torque improvement merits specific attention in the context of the e-rickshaw application. The torque distortion observed under fixed duty cycle operation — attributable to irregular power delivery from a sub-MPP PEMFC operating point — represents not merely an abstract power quality metric but a tangible source of mechanical vibration, acoustic noise, and passenger discomfort in a commercial rickshaw service environment. The neural network controller, by stabilising the PEMFC operating point through continuous duty cycle adaptation, substantially reduces this distortion — a practically significant improvement beyond efficiency metrics alone.

The observed reduction in stator current harmonic content under neural network control further translates to reduced I^2R copper losses in motor windings, lower core loss excitation, and extended winding insulation lifetime — all of which contribute to reduced maintenance intervals and total cost of ownership for commercial e-rickshaw operators .

IX. CONCLUSION

This investigation has demonstrated the performance advantages of a neural network-based adaptive power management strategy, implemented through a six-phase interleaved boost converter, for PEMFC-powered electric rickshaw propulsion. The principal findings are summarised as follows:

1) The six-phase interleaved boost converter achieves a measured voltage conversion gain of 8.39 with a theoretical 83.3% input current ripple attenuation, providing substantially superior membrane protection compared to single-phase and three-phase alternatives.

2) The Function Fitting Neural Network (fitnet, Levenberg-Marquardt, 3×10 neurons) power management controller improves PEMFC stack efficiency from 42.65% to 78.54% (+84.1%) by dynamically tracking the fuel cell maximum power point in response to real-time terminal voltage and current measurements.

3) Neural network control measurably reduces electromagnetic torque distortion and stator current harmonic ripple relative to fixed duty cycle operation, translating to improved ride quality, reduced acoustic noise, lower copper losses, and extended motor lifetime in the e-rickshaw service environment.

4) Hall effect sensor-based six-step commutation with PI speed regulation achieves stable BLDC motor operation across the complete e-rickshaw driving cycle in both operating modes, confirming the architectural independence and modularity of the motor drive system.

5) Future research directions include: experimental hardware validation using a DSP-based real-time controller, integration of a supercapacitor for peak power buffering and regenerative braking energy recovery, and investigation of deep learning architectures for improved MPPT generalisation under degraded PEMFC conditions.

REFERENCES

[1] Society of Manufacturers of Electric Vehicles (SMEV), “EV Sector Report 2023–24,” New Delhi, India, 2024.
[2] N. Mebarki, T. Rekioua, Z. Mokrani, D. Rekioua, and S. Bacha, “PEM fuel cell/battery storage system supplying electric vehicle,” Int. J. Hydrogen Energy, vol. 41, no. 45, pp. 20993–21005, 2016.
[3] S. Rafikiran, G. Devadasu, C. H. Basha, P. M. Tom, V. Prashanth, C. Dhanamjayulu, A. Kumbhar, and S. M. Muyeen, “Design and performance analysis of hybrid MPPT controllers for fuel cell fed DC-DC converter systems,” Energy Rep., vol. 9, pp. 4960–4970, 2023.
[4] K. J. Reddy and N. Sudhakar, “High voltage gain interleaved boost converter with neural network based MPPT controller for fuel cell based electric vehicle applications,” IEEE Access, vol. 6, pp. 3899–3908, 2018.
[5] K. J. Reddy and N. Sudhakar, “ANFIS-MPPT control algorithm for a PEMFC system used in electric vehicle applications,” Int. J. Hydrogen Energy, vol. 44, no. 29, pp. 15355–15369, 2019.
[6] Ballard Power Systems, “NEXA Power Module User’s Manual,” MAN5100078, 2003.
[7] A. Peer Mohamed and K. R. M. Vijaya Chandrakala, “Implementation of high step-up converter using RBFN MPPT controller for fuel cell based electric vehicle application,” Sci. Rep., vol. 14, p. 29364, Nov. 2024.
[8] A. Intidam, N. Ouanjli, A. Mahfoud, M. Al-Dhaifallah, M. El Mahfoud, and R. M. Bajaj, “Development and experimental implementation of optimized PI-ANFIS controller for speed control of brushless DC motor in fuel cell electric vehicles,” Energies, vol. 16, no. 4, p. 1693, 2023.
[9] R. Subbulakshmy, R. Palanisamy, S. Alshahrani, and C. Ahamed Saleel, “Implementation of non-isolated high gain interleaved DC-DC converter for fuel cell electric vehicle using ANN-based MPPT controller,” Sustainability, vol. 16, no. 3, p. 1335, Feb. 2024.
[10] D. Mane, P. Puranik, and A. Kulkarni, “Design and analysis of electric rickshaw powertrain for Indian urban conditions,” in Proc. IEEE PESGRE, Trivandrum, India, 2022, pp. 1–6.
[11] T. Selmi, A. Khadhraoui, and A. Cherif, “Fuel cell-based electric vehicles technologies and challenges,” Environ. Sci. Pollut. Res., vol. 29, pp. 78121–78131, 2022.

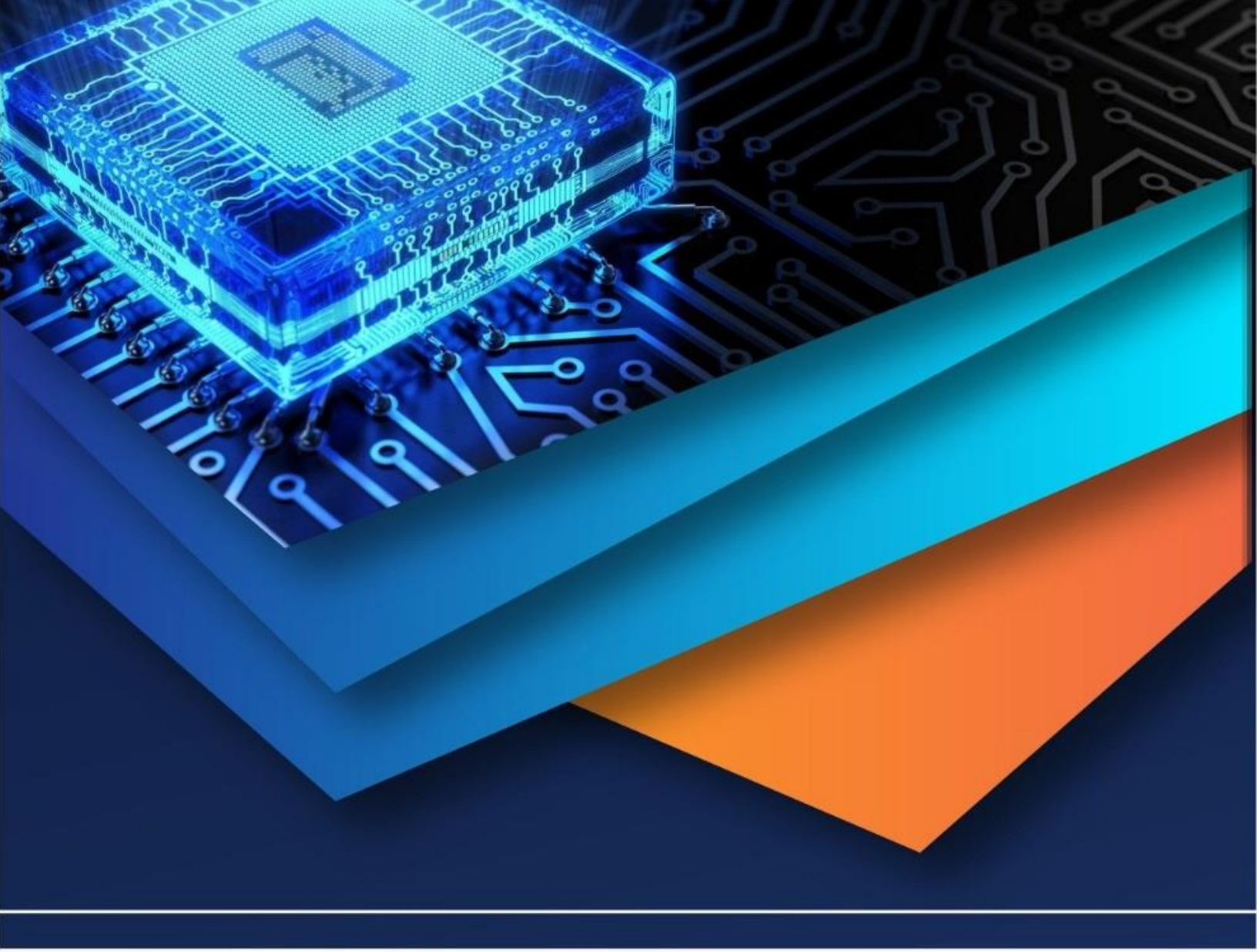

10.22214/IJRASET

45.98

IMPACT FACTOR: 7.129

IMPACT FACTOR: 7.429

INTERNATIONAL JOURNAL FOR RESEARCH

IN APPLIED SCIENCE & ENGINEERING TECHNOLOGY